ACS APPLIED MATERIALS & INTERFACES

Research Article

www.acsami.org

Controlling the Dopant Dose in Silicon by Mixed-Monolayer Doping

Liang Ye,[†,‡] Sidharam P. Pujari,[§] Han Zuilhof,[§,∥] Tibor Kudernac,[†] Michel P. de Jong,[‡] Wilfred G. van der Wiel,[‡] and Jurriaan Huskens*,[†]

[†]Molecular NanoFabrication group, MESA[+] Institute for Nanotechnology and [‡]NanoElectronics Group, MESA[+] Institute for Nanotechnology, University of Twente, P.O. Box 217, 7500 AE Enschede, The Netherlands

[§]Laboratory for Organic Chemistry, Wageningen University, Dreijenplein 8, 6703 HB Wageningen, The Netherlands

[∥]Department of Chemical and Materials Engineering, King Abdulaziz University, Jeddah, Saudi Arabia

ABSTRACT: Molecular monolayer doping (MLD) presents an alternative to achieve doping of silicon in a nondestructive way and holds potential for realizing ultrashallow junctions and doping of nonplanar surfaces. Here, we report the mixing of dopant-containing alkenes with alkenes that lack this functionality at various ratios to control the dopant concentration in the resulting monolayer and concomitantly the dopant dose in the silicon substrate. The mixed monolayers were grafted onto hydrogen-terminated silicon using well-established hydrosilylation chemistry. Contact angle measurements, X-ray photon spectroscopy (XPS) on the boron-containing monolayers, and Auger electron spectroscopy on the phosphorus-containing monolayers show clear trends as a function of the dopant-containing alkene concentration. Dynamic secondary-ion mass spectroscopy (D-SIMS) and Van der Pauw resistance measurements on the in-diffused samples show an effective tuning of the doping concentration in silicon.

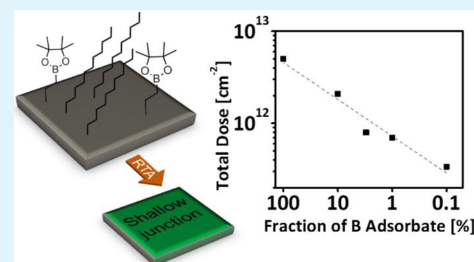

KEYWORDS: *monolayer doping, mixed monolayers, silicon, doping dose, electrical, organic*

INTRODUCTION

Downscaling of electronic devices is driven by performance improvement and cost reduction.[1,2] For decades, the semiconductor industry has been shrinking electronic components to keep up with Moore's Law. Doping of silicon is one of the key processes to tune its electrical properties by intentionally incorporating foreign atoms into the crystal lattice.[3] Conventional doping relies on ion implantation, which involves bombarding the material with high-energy, dopant-containing ions.[3] The advantage of this technique is its independent control of doping concentration and junction depth or doping profile.[4] However, ion implantation suffers from various drawbacks including damage to the crystal lattice during ion bombardment and subsequent transient-enhanced diffusion of the dopants caused by these defects.[5] This limits the application of this technique in making ultrashallow junctions,[6] which are used to suppress short channel effects merged with the downscaling of transistors. Alternative approaches to doping include solid-phase diffusion. However, this technique faces limits at controlling the doping concentration, especially near the surface. These drawbacks constitute a great challenge for further downscaling silicon devices.

The recently developed molecular monolayer doping (MLD) technique offers a promising alternative.[7] This technique utilizes hydrosilylation[8−12] to covalently attach dopant-containing molecules to hydrogen-terminated silicon. The dopants are subsequently driven in by a high-temperature annealing process. Compared to ion implantation, it is a milder technique to introduce dopants into a material and thus avoids crystal damage. Furthermore, this technique has the potential to dope 3-D structures on nonplanar silicon surfaces, which are more vulnerable to crystal damage.[13] Using MLD, dopants can be introduced into the material from the sidewalls, as well as from the top on such surfaces. Furthermore, sub-5 nm junctions have been demonstrated to date,[14] making MLD ideally suited for producing ultrashallow junctions. Localized doping on silicon has been shown by combining MLD with nanopatterning techniques such as nanoimprint lithography, achieving doped dot or line patterns on silicon.[15,16] While the control of junction depth and localized doping have been established with MLD, precise control of the amount of dopant or doping dose remains challenging.

Currently achieved doping concentrations with MLD are on the order of 10^{20} cm^{-3}. On the other hand, in the semiconductor industry the doping of silicon ranges from as low as parts per billion level up to a few percent, which is in the range of 10^{15}−10^{21} cm^{-3}. We believe that extending the doping concentration of MLD to a broader range will greatly expand its potential, especially in electronics and solar energy collection. Here, we report a technique in which a monolayer, consisting of a dopant-containing compound and the dopant-free 1-undecene, is grafted onto the silicon surface. The 1-undecene reacts with H−Si sites, hence reducing the ones available for the dopant-containing molecule. This reduces the amount of

Received: November 12, 2014
Accepted: January 21, 2015
Published: January 21, 2015

© 2015 American Chemical Society

DOI: 10.1021/am5079368
ACS Appl. Mater. Interfaces 2015, 7, 3231−3236

dopant atoms available for incorporation in the silicon crystal lattice during the annealing process. Although initial attempts were pioneered by Javey et al.,[7] the use of only two mixing ratios (1:5 and 1:20) with boron doping prevented a clear establishment of the validity of this method to reproducibly control the doping dose. Here we present a detailed study on the relation between the mixing ratio in solution, the monolayer composition resulting on the surface, and the doping dose inside the silicon upon thermal annealing for both boron and phosphorus doping using X-ray photoelectron spectroscopy (XPS), Auger electron spectroscopy (AES), dynamic secondary-ion mass spectroscopy (D-SIMS), and Van der Pauw measurements.

■ RESULTS AND DISCUSSION

Preparation of the samples is schematically shown in Scheme 1. In MLD, we used allylboronic acid pinacol ester (ABAPE) and diethyl vinylphosphonate (DVP) with olefin terminal groups as the dopant source. Piranha cleaning and HF etching provides the hydrogen-terminated silicon surface. Molecules were grafted onto the surface by hydrosilylation using mixtures of dopant-containing alkene and 1-undecene at various mixing ratios from 100% (pure dopant compound) to 0.1%. A capping layer of 50 nm SiO_2 was deposited on top to prevent the dopant atoms from being released to the ambient during the subsequent annealing step. The surface junction was achieved after high-temperature annealing at 1000 °C for 5 min, followed by removal of the capping layer in 1% aqueous HF.

Scheme 1. Preparation Process of the Mixed Monolayer Doping Samples[a]

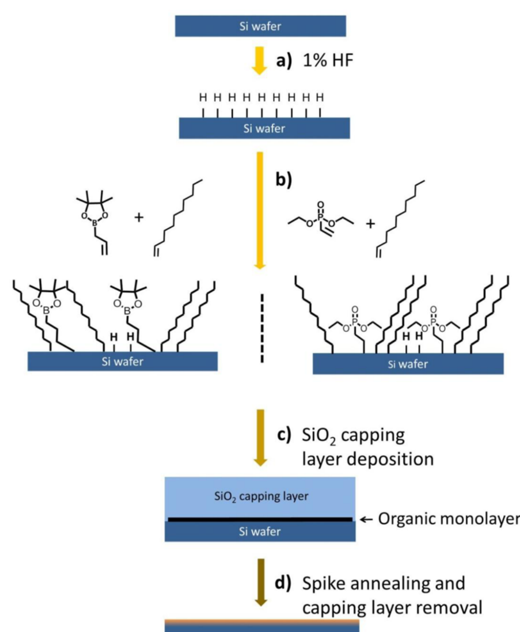

[a](a) Wet etching of native SiO_2 with dilute aqueous HF yields the H-terminated silicon surface, (b) hydrosilylation grafts dopant as well as diluting molecules onto the H-terminated Si surface, (c) SiO_2 capping layer is sputtered onto the modified surface, and (d) high-temperature rapid annealing and removal of capping layer result in a surface junction with dopants.

Following the hydrosilylation reaction, the substrates were first characterized by water contact angle (CA) measurements. The difference in wettability of the dopant-containing molecules and 1-undecene and their ratio will cause different CAs to be measured. The results are shown in Figure 1. ABAPE (boron) and DVP (phosphorus) contain a more hydrophilic headgroup compared to 1-undecene. The advancing/receding CAs for the monolayers formed by neat ABAPE and DVP start at low CA and increase when diluted with an increasing amount of undecene. This increase of the CA is observed up to the value of approximately 105/85, where it becomes constant with an increasing amount of undecene. This value corresponds to the reported value for alkene monolayers on silicon.[17] The plateau is reached for monolayers formed from mixed solutions containing 30% ABAPE and 10% DVP as shown in Figure 1a and 1b, respectively. At lower fractions of dopant adsorbate, the CA is not sensitive anymore to changes in the composition. This trend can be explained by Cassie's law, which predicts the CA on a composite surface, θ_c, based on the CAs on each of the two components and fractions of the two components

$$\cos \theta_c = f_1 \cos \theta_1 + f_2 \cos \theta_2$$

where θ_1 and θ_2 are the CAs observed for the two components separately. With this equation and the measured advancing/receding CAs of neat ABAPE, DVP, and 1-undecene monolayers of 77.6/54, 54.5/0, and 105/88, we calculated the predicted CAs for both ABAPE and DVP mixed surface. The calculated data are shown as dashed lines in Figure 1. The measured CAs fit well with the calculated ones, which indicates that the fraction of ABAPE and DVP in the mixed monolayers with 1-undecene is in a good agreement with their amounts present in the solutions. The slight overestimation of the CA of the DVP mixed monolayers (Figure 1b) may indicate a small preference for the binding of DVP relative to 1-undecene in this case.

To get quantitative results on the composition of the mixed monolayers, samples with ABAPE monolayers were investigated by X-ray photoelectron spectroscopy (XPS). The measurements were performed at a 20° takeoff angle to achieve a higher relative boron signal intensity. Figure 2a shows a spectrum acquired on a full ABAPE monolayer. The boron signal at 191.6 eV partially overlaps with the Si 2s plasmon signal. The higher energy edge of the Si 2s plasmon was used as tilted background (red line in Figure 2a) in the quantification. Figure 2b shows the C 1s region in which the two peaks at 284.8 and 286.8 eV correspond to C−C and C−O bonding in the molecules, respectively. The ratio of the two peak areas was calculated to be 3.3, close to the theoretical 3.5 deducted from the atomic ratio of ABAPE ($C_9H_{17}O_2B$). Relative boron and carbon fractions as well as the boron to carbon ratio were calculated for the monolayers prepared at different fractions of dopant adsorbate in solution (see Table 1). The measured relative boron fraction decreases dramatically from 1.09% for the monolayer prepared with the neat compound to about 0.01% for the monolayer prepared at 6% of ABAPE. The latter approaches the detection limit of the instrument, and lower amounts of boron could not be unambiguously detected. The measured carbon fraction, on the other hand, increased as more 1-undecene was added into the monolayers. We note that from the pure compound (100% ABAPE) a B/C ratio of 0.03 is measured, which is lower than the theoretical 0.11 deducted from the atomic ratio of ABAPE. This could be attributed to unintended carbon contamination from the ambient. Given that all samples were prepared and measured under the same conditions, implying similar amounts of contamination, the

DOI: 10.1021/am5079368
ACS Appl. Mater. Interfaces 2015, 7, 3231−3236

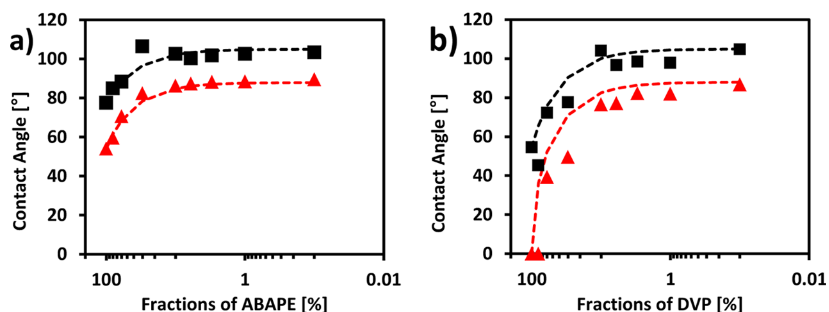

Figure 1. Contact angle measurements of silicon substrates functionalized with mixed monolayers of allylboronic acid pinacol ester (ABAPE, a) or diethyl vinylphosphonate (DVP, b) and 1-undecene as a function of the fraction of dopant adsorbate in solution. Advancing (■) and receding (▲) contact angles are shown separately. Predicted CAs based on Cassie's law are shown as dashed lines.

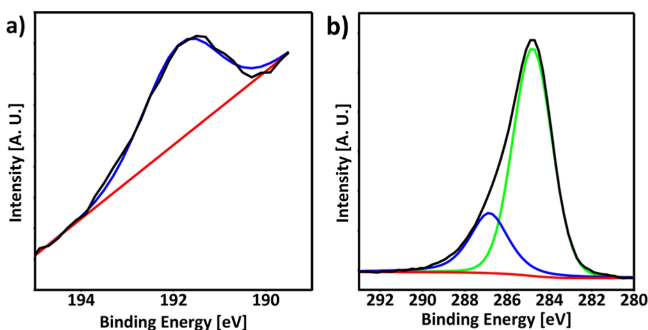

Figure 2. XPS spectrum at 20° takeoff angle of the B 1s (a) and C 1s (b) regions for a full monolayer of ABAPE. Due to partial overlap with the Si 2s plasmon peak, a tilted baseline (red) was used for quantification. Two carbon peaks at 284.8 (green) and 286.8 eV (blue) are attributed to C−C and C−O bonding, respectively.

Table 1. Relative Boron and Carbon Concentrations and Boron to Carbon Ratio from XPS Measurements on Surfaces Modified with Mixed Monolayers with ABAPE and 1-Undecene

sample	B [%]	C [%]	B/C
100% ABAPE	1.09 ± 0.17	34.05	0.0320 ± 0.0050
80% ABAPE	0.69 ± 0.32	40.75	0.0169 ± 0.0078
60% ABAPE	0.68 ± 0.13	47.71	0.0142 ± 0.0027
30% ABAPE	0.14 ± 0.12	45.73	0.0031 ± 0.0026
10% ABAPE	0.06 ± 0.12	51.53	0.0012 ± 0.0023
6% ABAPE	0.01 ± 0.01	51.07	0.0002 ± 0.0002

variations over the series can nevertheless be determined reliably.

Because of the overlap of the phosphorus P 2p signal with the Si 2p plasmon peak, we were unable to establish the amount of DVP on silicon by means of XPS. Alternatively, Auger electron spectroscopy (AES) was performed on those samples. A full AES spectrum of the 100% DVP sample is shown in Figure 3a. Signals of phosphorus, carbon, oxygen, and silicon can be detected in the full spectrum scan. Figure 3b shows the quantification of the amount of phosphorus measured on monolayers prepared at different fractions of DVP. Two locations on each sample were measured. All samples were measured under the same conditions, with the same instrumental settings to make sure that the sample-to-sample trend could be determined reliably. The measured phosphorus concentration decreases from about 1.7% to about 0.5% as the DVP fraction varies from 100% to 10%. The phosphorus signal leveled off at DVP fractions below 6%.

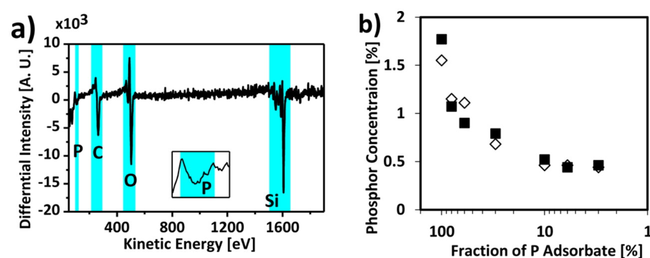

Figure 3. (a) Full differentiated AES spectrum on a pure DVP monolayer sample. P, C, O, and Si can be identified from this spectrum. (Inset) Zoomed in region of P. (b) Relative amount of P plotted as a function of the DVP fraction in the mixture used to make the monolayers. Two points were measured on each sample (■ and ◇).

Overall, both the XPS (boron) and the AES (phosphorus) data confirmed that mixing the dopant adsorbate with 1-undecene provides mixed monolayers on the surfaces. We also tried to measure ABAPE samples using AES; however, the instrument's detection limit for boron prevented us from drawing any firm conclusion from the data. Even though both data do not give well quantified results, the relative trends indicate a roughly linear relationship between the fraction of dopant adsorbate and its presence in the mixed monolayer in both dopant cases, in agreement with the CA data presented above.

In order to diffuse the doping atoms into the underlying silicon substrate, a SiO_2 capping layer of 50 nm was sputtered on top to prevent the monolayer to be disintegrated and removed from the substrate during the rapid thermal annealing step. The diffusivity of boron and phosphorus is considerably higher in silicon than in silicon oxide.[18,19] The samples were annealed at 1000 °C for 5 min during which the molecules forming the monolayer decompose and the formed elements diffuse into the silicon.

To study the diffusion process, the capping layer was removed and dynamic secondary ion mass spectroscopy (D-SIMS) was used to measure the depth profiles of the diffused elements (Figure 4a and 4b). The dopant profiles follow the diffusion profile by Fick's law. For boron-doped samples, the dopants diffuse to a depth of about 125 nm for the pure compound. The diffusion depth gradually decreases to 50 nm for the 0.1% boron-containing adsorbate. The surface concentration reaches 1.6×10^{19} cm^{-3} for the pure compound, and this concentration decreases to 4.2×10^{18} cm^{-3} for the 0.1% diluted adsorbate. For phosphorus-doped samples, the measured diffusion depth also varied from about 150 nm for the pure compound to 50 nm for the 0.1% phosphorus-

DOI: 10.1021/am5079368
ACS Appl. Mater. Interfaces 2015, 7, 3231−3236

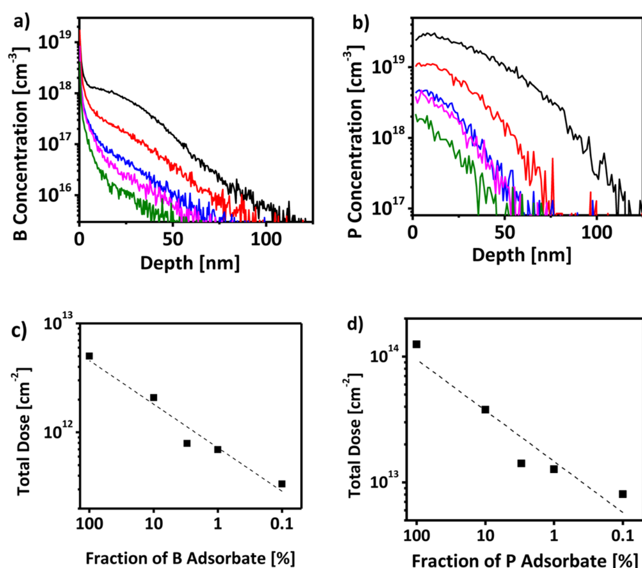

Figure 4. Dynamic SIMS dopant profiles of (a) boron- and (b) phosphorus-doped surface junctions after capping layer deposition and high-temperature annealing. Black, red, blue, magenta, and green lines show the doping profile of 100%, 10%, 3%, 1%, and 0.1% mixing ratios, respectively. (c and d) Total dose of dopant per cm^{-2}; dashed line indicates the decreasing trend with the fraction of adsorbate. All concentration and total dose measurements have an error below 10%.

containing adsorbate. The surface concentration varied from 2.4×10^{19} to 2.2×10^{18} cm^{-3}. These data effectively show that mixing the dopant molecules with 1-undecene can tune the doping concentration. Lower concentrations can be achieved by further diluting the adsorbate in the hydrosilylation process. The areal doses of dopant per cm^{-2} were calculated by integrating the concentration over depth as shown in Figure 4c and 4d. For both the boron- and the phosphorus-doped cases the total dose was reduced by a factor between 2 and 3 as the mixing ratio decreased by 1 order of magnitude. This result deviates from the fractions in the monolayer prior to diffusion of the dopant atom into silicon and the contact angle measurements done before on the monolayers. We observed that at lower concentrations within the monolayer the dopants are more efficiently diffused. Multiple reasons can contribute to this behavior as the diffusion of the atoms from the monolayer into the silicon is a complex process and depends on the decomposition kinetics of the molecules, solubility, and diffusivity of the specific elements in Si and SiO_2 and the related interfacial effects. Although the diffusivity of the dopants in Si is considerably higher than their diffusivity in SiO_2 it still remains unclear how much of the dopants is lost in the capping layer. Even though the diffusion process is nonlinear, our data show that the doping dose can be tuned in a controlled manner over an order of magnitude by changing the ratio between dopant adsorbate and 1-undecene for both P and B doping (Figure 4c and 4d).

Since the doping utilizes organic precursors, incorporation of carbon is potentially problematic in this process. The boron- and phosphorus-containing molecules have nine and six carbon atoms in their structures, while the undecene molecule has 11. The total amount of carbon could therefore be expected to be an order of magnitude higher than the dopant. We attempted to measure the carbon profile using SIMS. Due to the presence of atmospheric carbon residues that cannot be removed completely, the detection limit of carbon is restricted by a background level of about 1×10^{18} cm^{-3}. Consequently, we were unable to measure reliably the carbon content in the samples. Previous studies suggest that carbon contamination in MLD is limited to a depth of a few nanometers close to the surface.[20] Moreover, based on previous measurements of leakage currents, it is well accepted that the incorporation of carbon into the silicon lattice is not of a major concern.[14]

To see how the amount of doping in the substrate affects the electrical properties, the sheet resistance of the doped junctions was measured using the four-point Van der Pauw method.[21] An estimate of the sheet resistance (R_S) can be calculated from the measured SIMS profile using the following relation

$$\frac{1}{R_S} = \int qN(x)\mu(x)\mathrm{d}x \quad (1)$$

where q is the electron/hole charge, $N(x)$ is the concentration profile as a function of depth x, and $\mu(x)$ is the carrier mobility which can be determined using Klaassen's model[22]

$$\mu(x) = \mu_{\min} + \frac{\mu_{\max} - \mu_{\min}}{1 + (N(x)/N_{\mathrm{ref1}})^{x_1}} \quad (2)$$

The measured and calculated R_S values are shown in Figure 5. Both sets of data follow the same trend: as the amount of dopant atoms decreases, the resistance of the silicon increases. Thus, qualitatively, we can conclude that controlling the monolayer doping dose provides a way to control the electrical properties of the substrate.

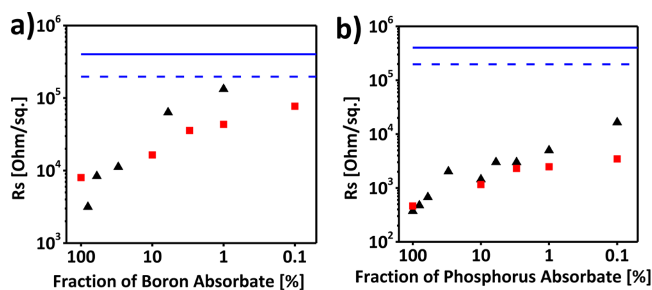

Figure 5. Sheet resistance measurements (▲) on (a) boron- and (b) phosphorus-doped samples as well as the estimated values (■) based on the doping profile measured by SIMS. Dashed and solid lines indicate the R_S measured on "carbon doped" and intrinsic Si without any doping. Standard deviations of all data points were found to be below 5%, apart from the 1% boron absorbate case, which has an error of 16%.

The measured R_S is in good agreement with the predicted one for phosphorus-doped samples. For the boron-doped ones, the measured R_S trend is steeper than the theoretical one but still in good agreement. As a control experiment a sample modified with pure 1-undecene and annealed under the same conditions was prepared and characterized as well. The resistance measured for this carbon-doped silicon substrate is shown in Figure 5 (dashed line). R_S of an intrinsic piece of Si without any modification was also measured and indicated as the solid line. The resistance of the carbon-doped sample, although lower than the intrinsic one, is still in the same order of magnitude. This indicates that the presence of carbon has a minor effect on the silicon resistance.

DOI: 10.1021/am5079368
ACS Appl. Mater. Interfaces 2015, 7, 3231−3236

CONCLUSIONS

We demonstrated tunable silicon doping using MLD for both p- and n-type dopants. The doping-containing precursor molecules are mixed with undecene and grafted onto the silicon surfaces by hydrosilylation to control the amount of dopants at the interface. A surface junction was formed by deposition of a capping layer and high-temperature annealing to drive in the dopant atoms. Measurements on both the modified surface and the in-diffused junctions showed that tuning of the doping level by mixing the monolayers is feasible. Water contact angle goniometry on the modified surface indicated that the monolayer composition is proportional to the fractions of doping-containing molecules in the solution. The surface concentrations achieved are 4.2×10^{18} cm^{-3} for boron-doped and 2.2×10^{18} cm^{-3} for phosphorus-doped silicon. Both the surface concentration and the doping dose can be varied over 1 order of magnitude. The high concentration measured at lower dopant atom fractions suggests a suppression of the dopant atom migration into the silicon at higher concentration. Further dilution of the boron or phosphorus adsorbate could in principle achieve a lower level of doping. We also demonstrated that the resistance of the samples correlates with the amount of dopants introduced via the monolayer. This shows that using mixed monolayers constitutes an important control parameter in the MLD technique and will dramatically enhance its potential use in the formation of nanoscale functional devices. It further underscores the general and high potential of molecular monolayers in achieving nanomaterials properties. The monolayer-doped substrates thus achieved may find application in nanoelectronic and solar energy-related devices.

MATERIALS AND METHODS

Monolayer Formation. Allylboronic acid pinacol ester (97%, ABAPE), diethyl vinylphosphonate (97%, DVP), 1-undecene (97%), and mesitylene (puriss, >99.0%) were ordered from Sigma-Aldrich and used as received. ABAPE or DVP were mixed with 1-undecene at various fractions from 100% (pure dopant molecule) to 0.1%. This precursor mixture was then diluted with mesitylene at a ratio of 1:19 v/v. The mixed chemicals were transported into a reaction flask and degassed using the freeze−pump−thaw method for at least three cycles. Single-side polished intrinsic silicon ⟨100⟩ wafers were diced into 1 × 1 cm pieces and cleaned in acetone sonication for 10 min to remove particles generated during dicing and then in Piranha (98% of H_2SO_4 and 30% H_2O_2 mixed at 3:1 v/v) for 30 min to remove any possible organic contaminant on the surface. Thereafter, the pieces were dipped in 1% aqueous HF to remove the native silicon oxide layer and yield a hydrogen-terminated surface. After rinsing in Milli-Q water (resistivity >18 MΩ·cm) and drying in a N_2 stream, the cleaned silicon pieces were transported into the reaction flask in a glovebox filled with nitrogen. Hydrosilylation, which grafts the chemical compounds onto the H−Si surface, was performed by heating the reaction flask equipped with a condenser up to 180 °C in an oil bath overnight under continuous nitrogen inflow. The reaction was stopped by removing the heating. The pieces were taken out, rinsed with an excessive amount of toluene (puriss), acetone (puriss), methanol (absolute), and Milli-Q water, and followed by sonication in acetone for 10 min to remove any physisorbed material. Contact angles were measured immediately after the hydrosilylation. Then the pieces were sealed in a nitrogen glovebox and stored under nitrogen prior to further measurements or high-temperature annealing.

XPS. XPS measurements were performed on a Physical Electronics Quantera scanning XPS setup. Monochromatic Al Kα X-rays at 1486.7 eV were used. The chamber was evacuated to below 3×10^{-9} Torr. Measurements were performed with argon neutralization, and the working pressure was maintained at around 2×10^{-8} Torr throughout the measurement. A takeoff angle of 20° and acceptance angle of 20 sr were used for collecting signals from the monolayers. Collected spectra were calibrated setting the C 1s peak at 284.8 eV.

AES. AES measurements were performed at room temperature with a scanning Auger electron spectroscope (JEOL Ltd. JAMP-9500F field emission scanning Auger microprobe) system. AES spectra were acquired with a primary beam of 10 keV. The takeoff angle of the instrument was 0°. We used the differential energy spectrum to subtract background from the direct Auger spectrum for calculating the peak-to-peak intensity. The first differential $d(N(E))/d(E)$ Auger spectra were obtained by numerical derivation of the direct $N(E)$ integrated Auger data displaying an absolute scale with counts/second units by a universal Savitzky−Golay (SG) Quadratic differential filter using seven points and used to calculate the peak-to-peak intensity of Auger electrons and derive the elemental compositions. The differential spectrum is simply the differential of the direct spectrum with respect to energy. All AES spectra were evaluated by CasaXPS software (version 2.3.16 Prerel 1.4). The spectra were calibrated with the carbon peak at 263.0 eV.

Capping Layer Deposition and Annealing. Fifty nanometers of SiO_2 was sputtered onto the monolayer-modified silicon surface using a custom-built sputtering system. The chamber was backfilled with 1 sccm of oxygen to achieve stoichiometric SiO_2 layers. The power applied on the target was 400 W, resulting in a deposition rate of 3.4 nm/min. High-temperature annealing was performed in a furnace set at 1000 °C for 5 min. After annealing, the samples were taken out and cooled down to room temperature.

SIMS Measurements. In-diffused samples were first dipped in HF to remove the capping layer and then cleaned with Piranha to remove any organic residuals from the surface. SIMS depth profiles were recorded using a Cameca IMS 6f system with 3 keV O_2^+ primary ions in positive mode. The error for all data was within 10% as determined from multiple measurements on different positions on the same sample. Secondary ions of ^{11}B and ^{31}P were detected. The measured ^{11}B concentration was converted to total boron coverage using the known isotopic ratio. The measurement chamber was backfilled with O_2. Quantification and depth calibration were based on reference samples with known profiles.

Sheet Resistance. The four-probe Van der Pauw method[21] was used to determine the sheet resistance of samples on a probe station. The current was swept between two neighboring connections, while the voltage was measured between the other two. The slope extracted from the measured $I-V$ curve gave the resistance. Swapping the current source and voltage measurement electrodes provides another measurement of the same resistance. The average of these two gave the resistance R_A. The resistance R_B was measured at rotated polarity using the same method. Sheet resistance R_S was then determined from the equation

$$e^{-\pi R_A/R_S} + e^{-\pi R_B/R_S} = 1$$

The two resistances used to calculate R_A and R_B were used separately to determine the standard deviation of the sheet resistance data.

AUTHOR INFORMATION

Corresponding Author

*E-mail: j.huskens@utwente.nl.

Notes

The authors declare no competing financial interest.

ACKNOWLEDGMENTS

We thank Jurgen van Berkum, Rick Elbersen, and Janneke Veerbeek for fruitful discussions. L.Y. and J.H. acknowledge the China Scholarship Council for financial support. S.P.P. and H.Z. gratefully acknowledge the Nanonext T6-C1.3 for funding of this research. W.v.d.W. acknowledges financial support from the European Research Council (ERC StG 240433).

REFERENCES

(1) Peercy, P. S. The Drive to Miniaturization. *Nature* **2000**, *406*, 1023−1026.

(2) Lundstrom, M. Moore's Law Forever? *Science* **2003**, *299*, 210−211.

(3) Jones, E. C.; Ishida, E. Shallow Junction Doping Technologies for Ulsi. *Mater. Sci. Eng. R: Rep.* **1998**, *24*, 1−80.

(4) Aleman, M.; Rosseel, E.; Van Wichelen, K.; Pawlak, B. J.; Janssens, T.; Dross, F.; Posthuma, N. E.; Poortmans, J. Ion Implantation as a Potential Alternative for the Formation of Front Surface Fields for Ibc Silicon Solar Cells. *IEEE Photovoltaic Spec. Conf., 35th* **2010**, 1291−1294.

(5) Stolk, P. A.; Gossmann, H. J.; Eaglesham, D. J.; Jacobson, D. C.; Rafferty, C. S.; Gilmer, G. H.; Jaraiz, M.; Poate, J. M.; Luftman, H. S.; Haynes, T. E. Physical Mechanisms of Transient Enhanced Dopant Diffusion in Ion-Implanted Silicon. *J. Appl. Phys.* **1997**, *81*, 6031−6050.

(6) Lee, J. W.; Sasaki, Y.; Cho, M. J.; Togo, M.; Boccardi, G.; Ritzenthaler, R.; Eneman, G.; Chiarella, T.; Brus, S.; Horiguchi, N.; Groeseneken, G.; Thean, A. Plasma Doping and Reduced Crystalline Damage for Conformally Doped Fin Field Effect Transistors. *Appl. Phys. Lett.* **2013**, *102*, 223508.

(7) Ho, J. C.; Yerushalmi, R.; Jacobson, Z. A.; Fan, Z.; Alley, R. L.; Javey, A. Controlled Nanoscale Doping of Semiconductors Via Molecular Monolayers. *Nat. Mater.* **2008**, *7*, 62−67.

(8) Choi, K.; Buriak, J. M. Hydrogermylation of Alkenes and Alkynes on Hydride-Terminated Ge(100) Surfaces. *Langmuir* **2000**, *16*, 7737−7741.

(9) Li, Y.; Calder, S.; Yaffe, O.; Cahen, D.; Haick, H.; Kronik, L.; Zuilhof, H. Hybrids of Organic Molecules and Flat, Oxide-Free Silicon: High-Density Monolayers, Electronic Properties, and Functionalization. *Langmuir* **2012**, *28*.

(10) Scheres, L.; Giesbers, M.; Zuilhof, H. Organic Monolayers onto Oxide-Free Silicon with Improved Surface Coverage: Alkynes Versus Alkenes. *Langmuir* **2010**, *26*, 4790−4795.

(11) Scheres, L.; Arafat, A.; Zuilhof, H. Self-Assembly of High-Quality Covalently Bound Organic Monolayers onto Silicon. *Langmuir* **2007**, *23*, 8343−8346.

(12) Buriak, J. M. Organometallic Chemistry on Silicon Surfaces: Formation of Functional Monolayers Bound through Si-C Bonds. *Chem. Commun.* **1999**, 1051−1060.

(13) Longo, R. C.; Cho, K.; Schmidt, W. G.; Chabal, Y. J.; Thissen, P. Monolayer Doping Via Phosphonic Acid Grafting on Silicon: Microscopic Insight from Infrared Spectroscopy and Density Functional Theory Calculations. *Adv. Funct. Mater.* **2013**, *23*, 3471−3477.

(14) Ho, J. C.; Yerushalmi, R.; Smith, G.; Majhi, P.; Bennett, J.; Halim, J.; Faifer, V. N.; Javey, A. Wafer-Scale, Sub-5 Nm Junction Formation by Monolayer Doping and Conventional Spike Annealing. *Nano Lett.* **2009**, *9*, 725−730.

(15) Voorthuijzen, W. P.; Yilmaz, M. D.; Gomez-Casado, A.; Jonkheijm, P.; van der Wiel, W. G.; Huskens, J. Direct Patterning of Covalent Organic Monolayers on Silicon Using Nanoimprint Lithography. *Langmuir* **2010**, *26*, 14210−14215.

(16) Voorthuijzen, W. P.; Yilmaz, M. D.; Naber, W. J. M.; Huskens, J.; van der Wiel, W. G. Local Doping of Silicon Using Nanoimprint Lithography and Molecular Monolayers. *Adv. Mater.* **2011**, *23*, 1346−1350.

(17) Sieval, A. B.; Vleeming, V.; Zuilhof, H.; Sudholter, E. J. R. An Improved Method for the Preparation of Organic Monolayers of 1-Alkenes on Hydrogen-Terminated Silicon Surfaces. *Langmuir* **1999**, *15*, 8288−8291.

(18) Fair, R. B. Concentration Profiles of Diffuse Dopants in Silicon. In *Impurity Dopant Processes in Silicon*; Yang, F. Y. Y., Ed.; North Holland: Amsterdam, 1981.

(19) Ghezzo, M.; Brown, D. M. Diffusivity Summary of B, Ga, P, As, and Sb in SiO_2. *J. Electrochem. Soc.* **1973**, *120*, 146−148.

(20) Shimizu, Y.; Takamizawa, H.; Inoue, K.; Yano, F.; Nagai, Y.; Lamagna, L.; Mazzeo, G.; Perego, M.; Prati, E. Behavior of Phosphorous and Contaminants from Molecular Doping Combined with a Conventional Spike Annealing Method. *Nanoscale* **2014**, *6*, 706−710.

(21) van der Pauw, L. J. A Method of Measuring the Resistivity and Hall Coefficient on Lamellae of Arbitrary Shape. *Philips Tech. Rev.* **1958**, *20*, 220−224.

(22) Klaassen, D. B. M. A Unified Mobility Model for Device Simulation—I. Model Equations and Concentration Dependence. *Solid-State Electron.* **1992**, *35*, 953−959.